NANO LETTERS

Letter

pubs.acs.org/NanoLett

Large-Gap Magnetic Topological Heterostructure Formed by Subsurface Incorporation of a Ferromagnetic Layer

Toru Hirahara,[*,†] Sergey V. Eremeev,[‡,¶,§,∥] Tetsuroh Shirasawa,[⊥] Yuma Okuyama,[†] Takayuki Kubo,[#] Ryosuke Nakanishi,[#] Ryota Akiyama,[#] Akari Takayama,[#] Tetsuya Hajiri,[○] Shin-ichiro Ideta,[○] Masaharu Matsunami,[○] Kazuki Sumida,[△] Koji Miyamoto,[▽] Yasumasa Takagi,[◆] Kiyohisa Tanaka,[○] Taichi Okuda,[▽] Toshihiko Yokoyama,[◆] Shin-ichi Kimura,[○] Shuji Hasegawa,[#] and Evgueni V. Chulkov[∥,▲,□,¶,§]

[†]Department of Physics, Tokyo Institute of Technology, Tokyo 152-8551, Japan

[‡]Institute of Strength Physics and Materials Science, Tomsk 634055, Russia

[¶]Tomsk State University, Tomsk 634050, Russia

[§]Saint Petersburg State University, Saint Petersburg 198504, Russia

[∥]Donostia International Physics Center (DIPC), Paseo de Manuel Lardizabal, 4, 20018 San Sebastián/Donostia, Basque Country, Spain

[⊥]Institute for Solid State Physics, University of Tokyo, Kashiwa 277-8581, Japan

[#]Department of Physics, University of Tokyo, Tokyo 113-0033, Japan

[○]UVSOR Facility, Institute for Molecular Science, Okazaki 444-8585, Japan

[△]Graduate School of Science, Hiroshima University, Higashi-Hiroshima 739-8526, Japan

[▽]Hiroshima Synchrotron Radiation Center, Hiroshima University, Higashi-Hiroshima 739-8526, Japan

[◆]Department of Materials Molecular Science, Institute for Molecular Science, Okazaki 444-8585, Japan

[▲]Departamento de Física de Materiales, Facultad de Ciencias Químicas, UPV/EHU, Apdo. 1072, 20080 San Sebastián, Basque Country, Spain

[□]Centro de Física de Materiales, CFM-MPC, Centro Mixto CSIC-UPV/EHU, Apdo.1072, 20080 San Sebastián/Donostia, Basque Country, Spain

Supporting Information

ABSTRACT: Inducing magnetism into topological insulators is intriguing for utilizing exotic phenomena such as the quantum anomalous Hall effect (QAHE) for technological applications. While most studies have focused on doping magnetic impurities to open a gap at the surface-state Dirac point, many undesirable effects have been reported to appear in some cases that makes it difficult to determine whether the gap opening is due to the time-reversal symmetry breaking or not. Furthermore, the realization of the QAHE has been limited to low temperatures. Here we have succeeded in generating a massive Dirac cone in a $MnBi_2Se_4/Bi_2Se_3$ heterostructure, which was fabricated by self-assembling a $MnBi_2Se_4$ layer on top of the Bi_2Se_3 surface as a result of the codeposition of Mn and Se. Our experimental results, supported by relativistic *ab initio* calculations, demonstrate that the fabricated $MnBi_2Se_4/Bi_2Se_3$ heterostructure shows ferromagnetism up to room temperature and a clear Dirac cone gap opening of ~100 meV without any other significant changes in the rest of the band structure. It can be considered as a result of the direct interaction of the surface Dirac cone and the magnetic layer rather than a magnetic proximity effect. This spontaneously formed self-assembled heterostructure with a massive Dirac spectrum, characterized by a nontrivial Chern number $C = -1$, has a potential to realize the QAHE at significantly higher temperatures than reported up to now and can serve as a platform for developing future "topotronics" devices.

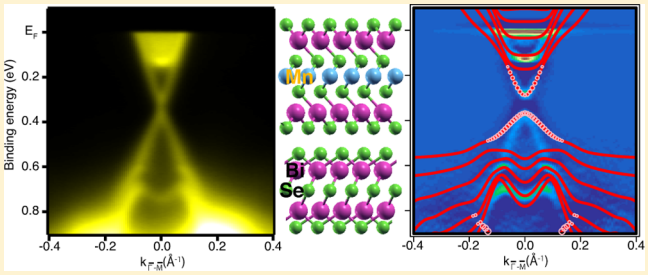

KEYWORDS: *Topological insulators, magnetism, massive Dirac cone, quantum anomalous Hall effect*

Classification of materials and phases based on the "topological properties" of the system has become one of the most extensively studied research fields in physics and

Received: February 10, 2017
Revised: May 11, 2017
Published: May 26, 2017

DOI: 10.1021/acs.nanolett.7b00560
Nano Lett. 2017, 17, 3493−3500

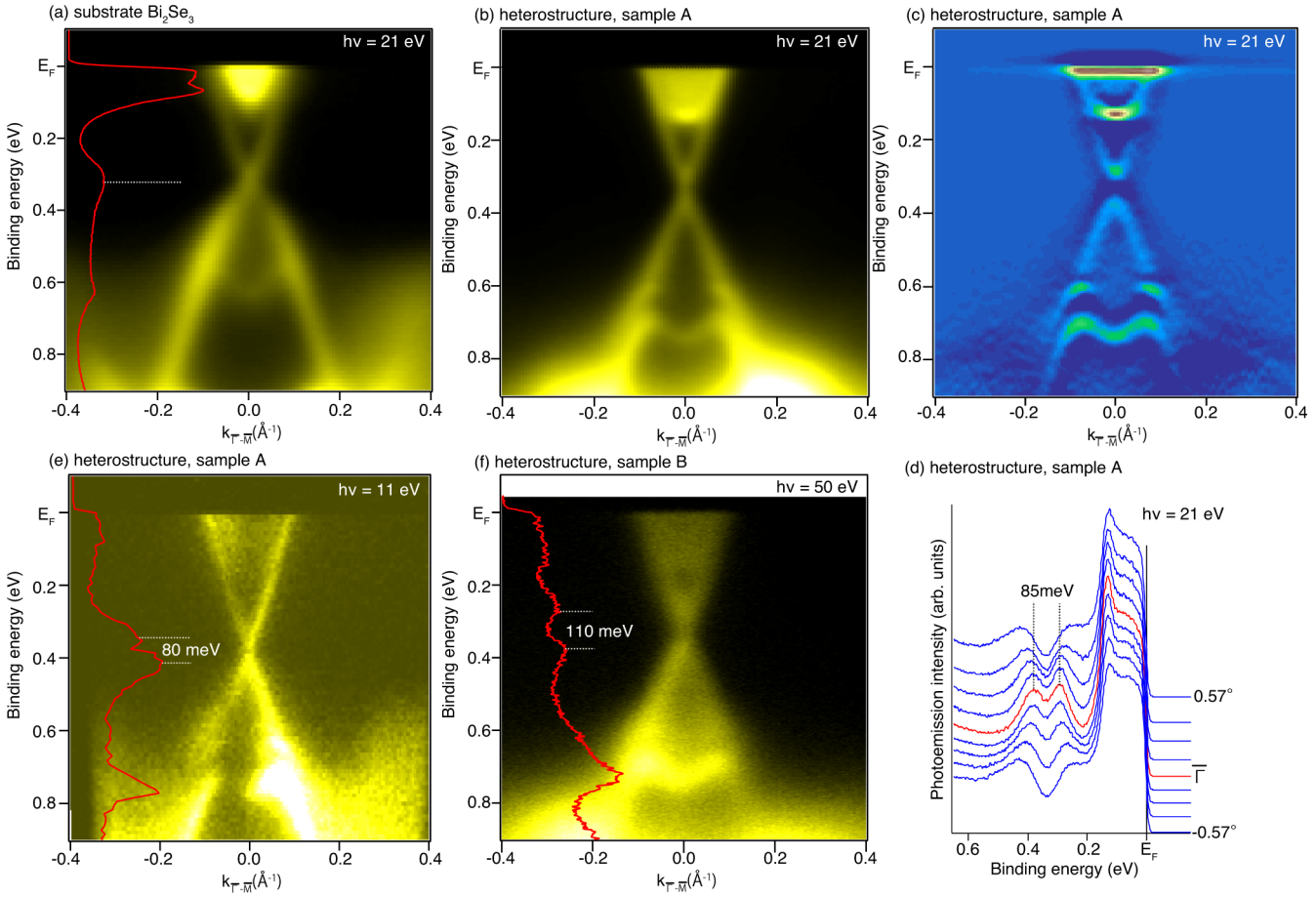

Figure 1. (a) Band dispersion of the substrate Bi_2Se_3 film measured along the $\bar{\Gamma}$–$\bar{M}$ direction taken at $h\nu$ = 21 eV. The red line shows the energy distribution curve (EDC) at the $\bar{\Gamma}$ point. (b) Band dispersion of the heterostructure for sample A measured along the $\bar{\Gamma}$–$\bar{M}$ direction taken at $h\nu$ = 21 eV. (c) The second derivative with respect to the energy of the band dispersion in (b). (d) Raw spectra (EDCs) near the $\bar{\Gamma}$ point of the band dispersion in (b). The gap size of the Dirac cone is 85 meV. (e) Band dispersion of the heterostructure for sample A measured along the $\bar{\Gamma}$–$\bar{M}$ direction taken at $h\nu$ = 11 eV. The gap size of the Dirac cone is 80 meV. The red line shows the EDC at the $\bar{\Gamma}$ point. (f) Band dispersion of the heterostructure for sample B measured along the $\bar{\Gamma}$–$\bar{M}$ direction taken at $h\nu$ = 50 eV. The gap size of the Dirac cone is 110 meV. The red line shows the EDC at the $\bar{\Gamma}$ point. All the measurements were performed at 30 K.

was the topic for the Nobel prize in physics in 2016.[1] Topological insulators (TIs) are insulating materials that have metallic surface states, whose electron spins are locked to their momentum.[2,3] In the simplest case, the surface states are helical Dirac Fermions and the Dirac point is robust due to the protection by time-reversal symmetry. When the time-reversal symmetry is broken in TIs, novel quantum phenomena have been predicted to occur including the formation of magnetic monopoles,[4] the quantum anomalous Hall effect (QAHE),[5] and the topological magnetoelectric effect.[6]

In terms of the electronic structure, a magnetic TI is expected to host a massive Dirac cone with a band gap. Many researches have been performed to induce magnetism in TIs by magnetic impurity doping when growing thin films.[7,8] Although it seemed that this was the most efficient way with the successful observation of the QAHE in Cr- or V-doped $(Bi,Sb)_2Te_3$ thin films,[8−10] the precise quantization of the Hall resistance at zero field is still only limited to low temperature (10−100 mK). The temperature for the realization of the QAHE (T_{QAHE}) depends on the Curie temperature as well as the size of the Dirac cone gap of the system. Up to now, the main obstacle in enhancing T_{QAHE} is an inhomogeneous distribution of magnetic atoms over the TI film that results in strong fluctuations of the magnetic energy gap.[11,12] Modulation doping was shown to increase T_{QAHE} and the QAHE was observed at 2 K for Cr-doped $(Bi,Sb)_2Te_3$ thin films when the magnetic-doped layer was placed 1 nm below the surface.[13] A recent theoretical work suggests that this can be enhanced by V and I codoping of Sb_2Te_3.[14]

Another drawback of the magnetically doped systems is that there has been no direct observation of the massive Dirac cone for the samples that show the QAHE using angle-resolved photoemission spectroscopy (ARPES).[15] With local probes such as scanning tunneling spectroscopy (STS), an inhomogeneous Dirac cone gap was observed for Cr-doped $(Bi,Sb)_2Te_3$.[11] However, for V-doped Sb_2Te_3, it was reported that impurity states will reside within the Dirac cone gap, and as a result, the density of states will look gapless.[16] Moreover, impurity bands will emerge near the Dirac point, and it was reported that a massive Dirac cone can arise even due to a nonmagnetic origin for impurity-doped Bi_2Se_3 films with ARPES.[17] Thus, one can say that magnetic impurity doped TI films are not promising in terms of (i) enhancing T_{QAHE} to the region where application becomes possible and (ii) clearly observing the gapped Dirac cone as a result of the time-reversal symmetry breaking in a macroscopic scale.

An alternative way to induce magnetism in TIs is to make a heterostructure of TIs and magnets. Such systems are also used

DOI: 10.1021/acs.nanolett.7b00560
Nano Lett. 2017, 17, 3493−3500

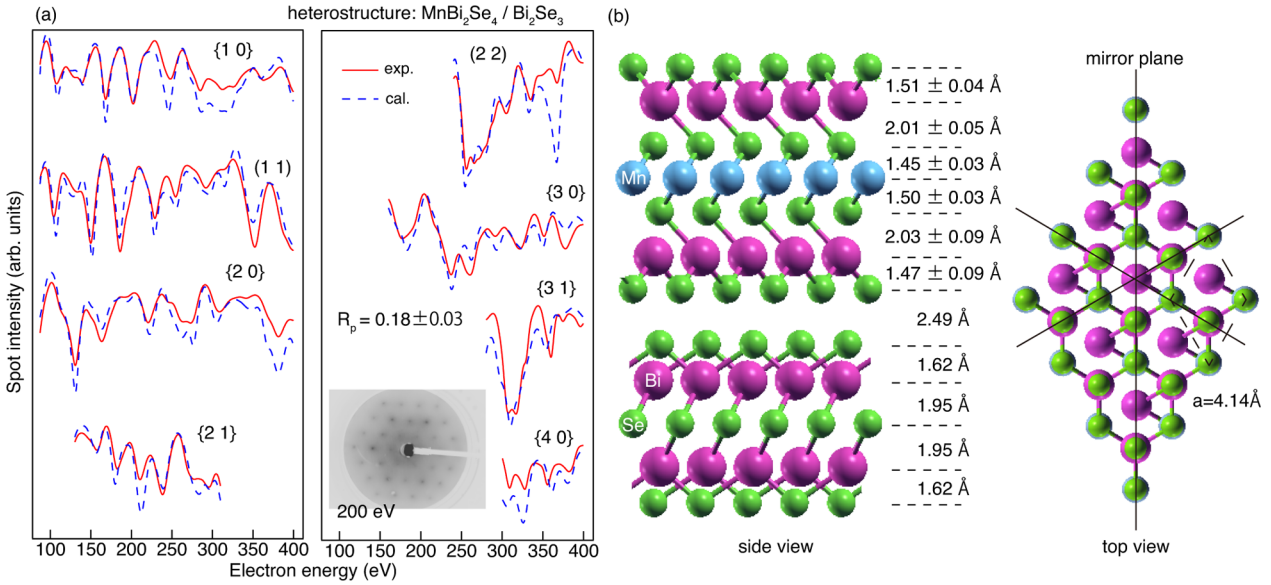

Figure 2. (a) Experimental *IV* spectra of LEED spots measured at 100 K for the heterostructure (red solid lines), and the calculated spectra of the optimized model shown in (b) (blue dotted lines). The inset shows the LEED pattern at 200 eV. (b) Cross-sectional (left) and top (right) view of the optimized model of the heterostructure, which turns out to be $MnBi_2Se_4/Bi_2Se_3$. Blue, pink, and green atoms represent Mn, Bi, and Se, respectively. The solid lines show the mirror plane and the dotted parallelogram shows the unit cell.

in experiments to observe the surface-state spin transport.[18−21] However, there has not been a direct observation of the QAHE as well as the existence of a gapped Dirac cone at the interfaces in these heterostructures. One reason for this is the absence an atomically sharp interface that makes the gap small and difficult to observe, which should be also responsible for the low spin-charge conversion efficiency. Even in some cases with a sharp interface (EuS/Bi_2Se_3), the Dirac cone gap was shown not to be related with the magnetic proximity effect,[22] although magnetization measurements showed evidence of a magnetic interaction.[23] In another case of $MnSe/Bi_2Se_3$, it was shown from *ab initio* calculations that states other than the gapped Dirac cone will cross E_F[24] and make the QAHE impossible to realize. However, the measured band structure was completely different from the calculation, but no clear explanation was given.[25] Thus, the interplay between the topological properties and magnetism in an ordered layered system needs to be examined further.

In the present study, we take advantage of self-organization to produce an ideal system of a magnetic insulator/TI heterostructure, which is formed spontaneously as a hexagonal $MnBi_2Se_4$ septuple layer (SL) on the basis of the topmost quintuple layer (QL) of Bi_2Se_3 film under Mn and Se codeposition. Due to the ferromagnetism of $MnBi_2Se_4$ up to room temperature as revealed by superconducting quantum interference device (SQUID) and X-ray magnetic circular dichroism (XMCD) measurements, the Dirac cone becomes massive with a gap size of ∼100 meV. First-principles calculations show that the calculated Chern number is $C = -1$, and the heterostructure is identified as a quantum anomalous Hall phase. Our results not only show the first example of a clear Dirac cone gap opening at the ferromagnet/TI interface but imply that this should be a suitable system to realize the QAHE at higher temperatures than previously reported by tuning the Fermi level as well as to develop novel devices based on the topological magnetoelectric effect.

Figure 1a shows the band dispersion of the Bi_2Se_3 thin film, which was used as the substrate for the heterostructure formation. The well-known Dirac cone of the surface states in the bulk band gap can be seen together with the bulk conduction band at the Fermi level due to the unintentional doping. The Dirac point is recognized as shown in the energy distribution curve (EDC) at the $\bar{\Gamma}$ point (red line). Figure 1b shows the band structure of the heterostructure (sample A) after Mn and Se were codeposited on Bi_2Se_3. It was measured immediately after cooling down the sample. A clear gap opening is observed at the Dirac point. This becomes more prominent by making the second derivative with respect to the energy of the image in Figure 1b, which is shown in Figure 1c. The gap size is deduced as ∼85 meV from the EDCs in Figure 1d. A slightly smaller gap is observed when the photon energy is changed to 11 eV, as shown in Figure 1e. The estimated gap size is ∼80 meV, which is nearly the same as that shown in Figure 1d. It can also be noticed that the midpoint of the energy gap has shifted down by about 70 meV from Figure 1b−d to Figure 1e, due to the band bending near the surface caused by the residual gas or defect formation[26,27] since Figure 1e was measured 12 h after Figure 1b−d. The band dispersion images taken with other photon energies for sample A are shown in Figure S1. Even though the gap exists irrespective of the Fermi level position, the gap size slightly changes depending on the measurement condition. However, there is no correlation between the midgap position and the gap size. Figure 1f shows the band dispersion image of a different sample (sample B) taken at $h\nu$ = 50 eV just after cooling down the sample posterior to the preparation. The gap size is ∼110 meV, larger than that for sample A although the midpoint of the gap is nearly the same. We have also measured the gap size for other samples, and the gap value is in the range of 75−120 meV when the Dirac point is located at the binding energy of 0.31−0.39 eV, although there is no correlation between the two quantities. We conclude that when Mn and Se are codeposited on Bi_2Se_3 and a heterostructure is formed, the Dirac cone becomes gapped. At first glance, it should be due to the magnetic proximity effect from antiferromagnetic MnSe.

DOI: 10.1021/acs.nanolett.7b00560
Nano Lett. 2017, 17, 3493−3500

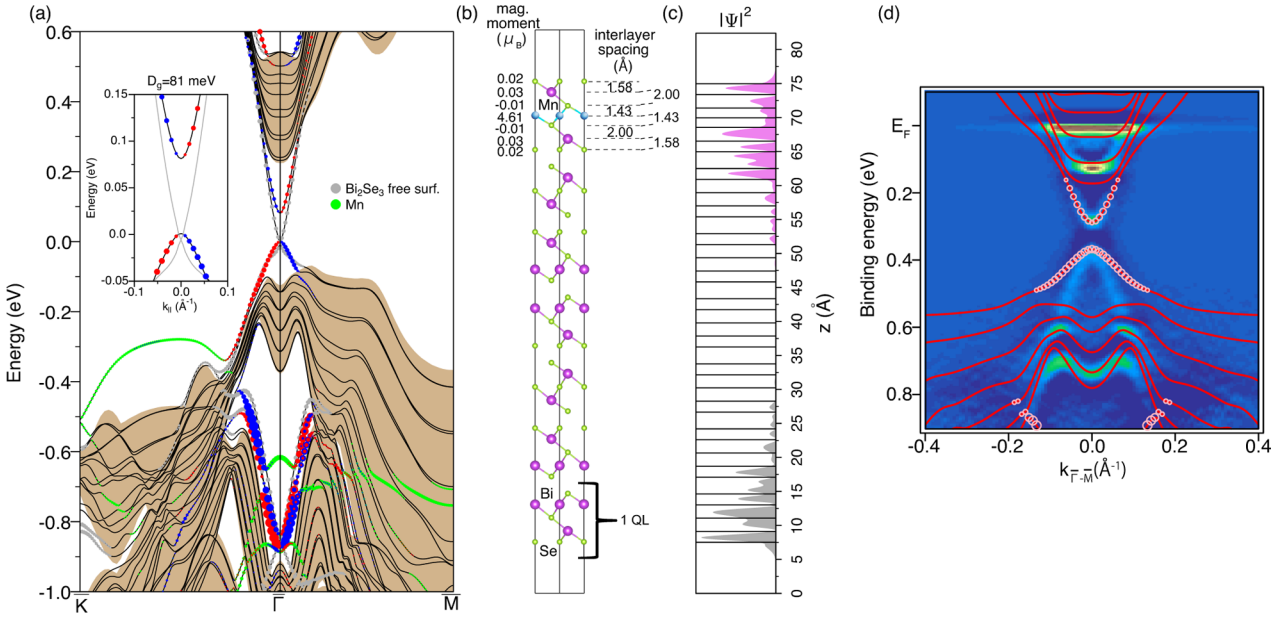

Figure 3. (a) Calculated band dispersion of a $MnBi_2Se_4$/6QL Bi_2Se_3 heterostructure. The states marked in red and blue are localized at the topmost SL and the next Bi_2Se_3 QL and spin-polarized in the in-plane direction perpendicular to the wavenumber (positive and negative, respectively). The states marked in green are the ones mostly localized at $MnBi_2Se_4$ SL and labeled "Mn". The states localized at the bottom surface of the slab are indicated in gray. The shaded area shows the bulk band projection of Bi_2Se_3. The inset shows a close-up of the Dirac state dispersion. A gap of 81 meV is found for the Dirac cone at the top surface. (b) The real space atomic configuration used in the calculation together with the interlayer spacings and layer-resolved magnetic moments. (c) Wave function ($|\Psi|^2$) plot for the gapped Dirac state at the top surface (violet) and that at the bottom surface (gray), respectively. (d) The calculated band dispersion overlapped with the experimental data of Figure 1c. Pink circles show the states localized in the SL.

However, there is one contradictory point about this band dispersion of the heterostructure. According to *ab initio* calculations,[24] the band dispersion of a $MnSe/Bi_2Se_3$ heterostructure should have the following characteristics: (i) a massive Dirac cone with a gap of 8.5 meV and (ii) other metallic states in the Bi_2Se_3 bulk band gap. In our experimental data, we do not find any additional states in the Dirac state energy region. Moreover, the gap size is an order of magnitude larger than that predicted in the calculation. Therefore, the calculation and the experiment are not consistent with each other. Various factors may be responsible for this inconsistency, such as the difference in the interface structure or the thickness of the MnSe layers. We have therefore performed structure analyses of the heterostructure based on the LEED *IV* technique to resolve this inconsistency.

Figure 2a shows the experimentally observed *IV* curves (red solid lines). To reproduce these curves, we have first assumed the $MnSe/Bi_2Se_3$ heterostructure that is expected from the sample preparation method. However, we could not obtain R-factor (R_p) values smaller than 0.4. Thus, it was proven that the heterostructure we have fabricated was not $MnSe/Bi_2Se_3$. We tried other structures and finally found one that was in striking agreement with the experimental LEED *IV* curves. The calculated *IV* curves for the optimized structure are shown by the blue-dotted lines in Figure 2a. The agreement between the two curves is excellent with $R_p = 0.18 \pm 0.03$. The structure thus determined is shown in Figure 2b. What is remarkable about this structure is that the deposited Mn and Se are not on top of the Bi_2Se_3 substrate, but they are incorporated inside the topmost QL of Bi_2Se_3. So we can say that a $MnBi_2Se_4$ SL spontaneously forms on top of Bi_2Se_3 by self-organization. Although the microscopic mechanism of MnSe bilayer immersion into the QL is not clear, our calculations show that the $MnBi_2Se_4$ SL is 630 meV energetically more favorable as compared to the MnSe bilayer (BL)/Bi_2Se_3 QL interface. $MnBi_2Se_4$ in the bulk form is reported to have the monoclinic structure with $C2/m$ symmetry. It is shown to be a narrow gap semiconductor and antiferromagnetic with $T_{Neel} \approx 14$ K.[28] However, the $MnBi_2Se_4$ SL that we have fabricated has a hexagonal structure and is a semiconductor with a gap of ~0.4 eV (Figure S3).

The electronic structure of the heterostructure was calculated based on the determined atomic structure of Figure 2b. Namely, a six QL film of Bi_2Se_3 was sandwiched between $MnBi_2Se_4$ and vacuum. The interlayer spacing values obtained after structural relaxation of the heterostructure and shown in Figure 3b are in excellent agreement with the experimentally determined values shown in Figure 2b. We found that the spin structure with the Mn magnetic moment pointing out-of-plane is 0.2 meV energetically more favorable than the one with in-plane spin polarization, and the magnetic moment of Mn was found to be 4.61 μ_B (Figure 3b). The calculated band dispersion is shown in Figure 3a. The red and blue points correspond to the states with in-plane spin polarization perpendicular to the wavenumber (positive and negative, respectively) that are localized at the topmost SL and the neighboring QL (refer to the Supporting Information for the experimental results of the Dirac cone spin-polarization). Near the Fermi level, the massless Dirac cone of pristine Bi_2Se_3 at the bottom surface can be found (gray points and gray line in inset) together with the massive Dirac state with a gap $D_g = 81$ meV at the top surface. The "gray" band can be a good reference for tracking the changes in the Dirac state. As can be seen, the lower part of the Dirac cone of the gapped state shows almost no change in the energy position, and the gap is formed by shifting up the upper branch. The calculations performed for a

DOI: 10.1021/acs.nanolett.7b00560
Nano Lett. 2017, 17, 3493−3500

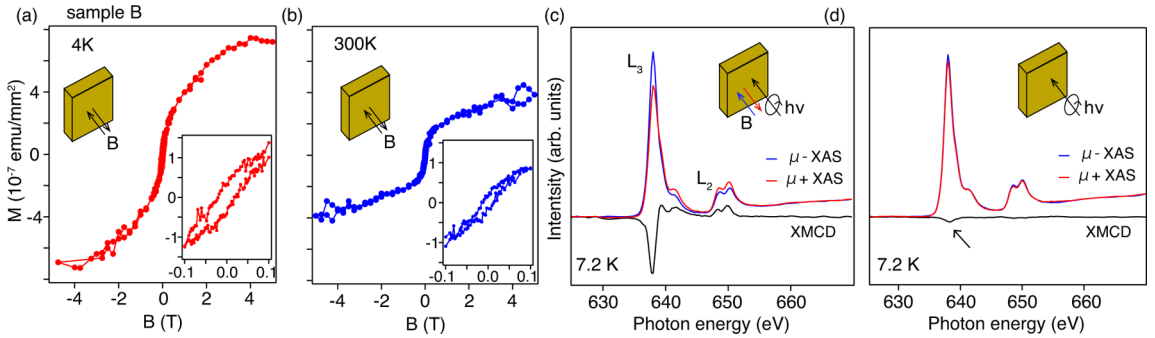

Figure 4. (a,b) Magnetization curves measured with SQUID for the Se-capped sample B taken at 4 K (a) and at 300 K (b), respectively. The magnetic field was applied perpendicular to the sample surface. The inset shows the close-up near zero-field. Clear hysteresis loops can be observed both at 4 and 300 K. (c) X-ray absorption spectra (XAS) at 7.2 K for a circularly polarized incident light when a ±5 T magnetic field was applied along the surface-normal direction. μ_+ and μ_- correspond to the spectrum obtained at +5 T and -5 T, respectively. The corresponding XMCD spectra is also shown. The Se capping layer was removed by annealing the sample in UHV. (d) Same as that in (c) but measured at zero field. A remanent XMCD signal can be observed (shown by the arrow).

symmetric heterostructure, where Bi_2Se_3 is sandwiched between two $MnBi_2Se_4$ SLs, result in the same value of the Dirac cone gap. Figure 3d shows this calculated spectrum overlapped with the experimental result (the calculation was rigidly shifted by −0.38 eV to fit to the experimental E_F). The agreement between the two is excellent with exception of flatter dispersion in the bottom part of the Dirac cone in the calculation whereas the gap size in the Dirac cone, as well as fine structures other than the Dirac cone, are reproduced. The green points in Figure 3a are states localized at the topmost SL and labeled "Mn" because it has the maximum contribution from the Mn p_z orbitals. They are located along the $\bar{\Gamma}$−$\bar{K}$ direction in the Bi_2Se_3 bulk band gap and a band that resembles this is also found in the calculated dispersion of the free-standing $MnBi_2Se_4$ SL (Figure S3). This was actually observed experimentally when we performed ARPES measurements along the $\bar{\Gamma}$−$\bar{K}$, as shown in Figure S9a. Altogether, the calculation reproduces the experimentally observed band structure nicely, and we are sure that the heterostructure we have fabricated is $MnBi_2Se_4/Bi_2Se_3$. Moreover, one can say that the mass acquisition of the Dirac cone is not due to a magnetic proximity effect because the Dirac state and the magnetic layer are both at the topmost SL (70% of the Dirac state is localized in the SL, see Figure 3c) We should rather say that this is a "direct interaction" between the magnetic layer and the surface Dirac cone, since they overlap in real space and some part of the wave-function of the Dirac cone is within the Mn layers. The original Dirac cone of Bi_2Se_3 has been pushed up to the newly formed $MnBi_2Se_4$ capping layer, which has been discussed previously for other topological-insulator based heterostructures.[29] This is the reason why there is a large gap of ∼80 meV at the Dirac point in contrast to the case of MnSe/Bi_2Se_3 where a magnetic proximity effect was considered.[24]

The gapped Dirac state has a potential to realize the QAHE. The quantized Hall conductance $\sigma_{yx} = Ce^2/h$ is related to the topological characteristic of the band structure known as the Chern number C.[30] Our calculations show that the gapped spectrum of the $MnBi_2Se_4/Bi_2Se_3$ heterostructure is characterized by the Chern number $C = -1$, which defines the obtained heterostructure unambiguously as a quantum anomalous Hall phase. To confirm the topological character of the heterostructure spectrum, we artificially decreased the spin−orbit interaction strength λ and found that it leads to the gap narrowing and its closing at $\lambda/\lambda_0 \approx 0.75$ (see Figure S4). Upon further decrease of the spin−orbit interaction strength, the gap reopens and the system becomes a topologically trivial insulator.

Next, we have tried to experimentally verify the absence of time-reversal symmetry in the heterostructure as the calculation suggests. Figure 4a,b shows the magnetization curves measured with SQUID for the Se-capped sample B taken at 4 K (a) and at 300 K (b), respectively. The magnetic field was applied perpendicular to the sample surface. (The data for the in-plane magnetization can be found in Figure S7). In order to display the situation near zero-field clearly, we show in the inset the close-up for −0.1 to 0.1 T. There is a vivid hysteresis loop both at 4 and 300 K, demonstrating the ferromagnetic nature of the heterostructure.[31] Actually, the gapped Dirac cone can also be observed at room temperature (Figure S2), and thus, the Curie temperature is confirmed to be above 300 K also from ARPES. We also performed XMCD measurements after removing the Se cap in UHV to make sure that the Se cap is not affecting the magnetic properties. Figure 4c shows the X-ray absorption (XAS) spectra at the Mn L edge measured at 7.2 K for a circularly polarized incident light when a ±5 T magnetic field was applied along the surface-normal direction. μ_+ and μ_- correspond to the spectrum obtained at +5 T and −5 T, respectively. The corresponding XMCD spectrum is also shown, and there is a clear signal. The quantitative analysis of the XMCD measurements using the sum-rule is discussed in the Supplementary Information, see Figure S5. The measurements were also performed at remanence (0 T applied magnetic field), namely, the signal was obtained after switching off the ±5 T magnetic field applied perpendicular to the surface (Figure 4d). Although weak (the peak at the L_3 edge is ∼7% compared to the data of Figure 4c), we still can notice the XMCD signal (the arrow in Figure 4d), and this confirms that the system is ferromagnetic. We believe that the SQUID data of Figure 4a,b and that obtained by XMCD in Figures 4c,d are both showing the ferromagnetism of the Mn layer despite the different probing depth of the two measurements since it can be the only source of ferromagnetism in the present heterostructure system.

The heterostructure we have fabricated demonstrates various advantages compared to previously studied quantum anomalous Hall systems. First, it forms spontaneously by depositing Mn and Se on top of Bi_2Se_3. We have done this using thin films, but in principle, it should also be possible to do this for single

DOI: 10.1021/acs.nanolett.7b00560
Nano Lett. 2017, 17, 3493−3500

crystals or even thinner films. This is in contrast to the extensively studied systems with an intentional magnetic impurity doping[7−9,16,17] in which fine-tuning of the impurity concentration is needed to achieve a long-range magnetic order.[32]

Second, in our samples, we have an ideal situation where the Dirac cone and the magnetic layer interact strongly due to the spatial overlap of the respective wave functions, thus leading to a large magnetic gap but with minimal effects on other bands. This is in contrast to heterostructures that utilize the magnetic proximity effect.[22−24]

Third, our samples are free from inhomogeneity since the structure was clearly determined by LEED measurements. This allowed us to observe a clear Dirac cone gap with ARPES and assign its origin unambiguously as due to the time-reversal symmetry breaking. Recalling that the presence of the impurity states makes it difficult to determine the gap opening in the Dirac cone as well as its origin,[16,17] this is a merit. Furthermore, the clear gap opening in ARPES means that our heterostructure does not show strong fluctuations of the magnetic energy gap.[11]

Finally, the Curie temperature of the heterostructure is above room temperature. Furthermore, the Dirac cone gap is larger than the thermal fluctuation at room temperature. Therefore, we can expect to observe the QAHE for our samples at higher temperatures than those previously reported[8−10] by moving the Fermi level into the induced gap either chemically[7] or by gating.[8,10,32] So our heterostructure may be used in application for developing "topotronics" devices.

Experimental and Calculation Methods. The heterostructure samples were prepared by molecular beam epitaxy in ultrahigh vacuum (UHV) chambers equipped with a reflection-high-energy electron diffraction (RHEED) system. First, a clean Si(111)-7 × 7 surface was prepared on an *n*-type substrate by a cycle of resistive heat treatments. The Si(111)β $\sqrt{3} \times \sqrt{3}$-Bi surface was formed by 1 ML (7.83×10^{14} cm^{-2}) of Bi deposition on the 7 × 7 surface at 620 K monitored by RHEED. Then Bi was deposited on the β $\sqrt{3} \times \sqrt{3}$-Bi structure at ∼200 °C in a Se-rich condition. Such a procedure is reported to result in a smooth epitaxial film formation with the stoichiometric ratio of Bi/Se = 2:3.[33,34] The grown Bi_2Se_3 films were annealed at ∼240 °C for 5 min. The thickness of the Bi_2Se_3 films in this work is ∼15 QL, which does not show the gap opening in the Dirac cone due to finite-size effects,[34,35] as shown in Figure 1a. Finally, Mn was deposited on Bi_2Se_3 in a Se-rich condition at ∼240 °C. As reported in ref 25, this results in a flat film formation, which was believed to be a heterostructure of MnSe/Bi_2Se_3.

ARPES and SARPES measurements were performed *in situ* after the sample preparation. The ARPES measurements were performed at BL-5U and 7U of UVSOR-III using *p*-polarized photons in the energy range of 30−65 and 7.5−28 eV, respectively.[36] All the data shown were taken at 30 K unless otherwise indicated. The energy and angular resolutions were 15 meV and 0.25°, respectively. The SARPES measurements were performed at BL-9B of HiSOR using *p*-polarized photons in the energy of 18−21 eV at 30 K.[37] In some of the measurements, a magnetic field as large as ∼0.1 T was applied to the sample. The energy and angular resolutions were 30 meV and 0.75°, respectively.

LEED measurements were also performed *in situ* after the sample formation in another UHV chamber. The LEED patterns with incident energy from 80 to 400 eV were recorded in steps of 1 eV by a digital CCD camera at 100 K. *IV* curves of 14 inequivalent diffraction spots were obtained. In order to determine the surface structure, we calculated the *IV* curves in the tensor LEED to fit the experimental *IV* curves using the SATLEED package of Barbieri/Van Hove[38] and minimized Pendry's R-factor (R_p). As shown in Figure 2b, each atomic layer was treated differently according to their environments. The in-plane lattice constant of the heterostructure was determined from positions of the LEED spots as well as the RHEED spots and was the same with that of Bi_2Se_3. Angular momentum up to 17 (l_{max} = 17) was taken into account because of the strong scattering of the heavy Bi atom (Z = 83). Considering the mean penetration depth of the incident electrons of ∼10 Å, only the topmost seven surface layers were allowed to relax, and we used the bulk Bi_2Se_3 parameters for the layers beneath. In search of the optimal structure, the Debye temperature of each atom was changed in steps of 10 K from 50 K up to 300 K. If MnSe grew on Bi_2Se_3, it should have the $p3m1$ symmetry. However, the symmetrically inequivalent spots, such as (1,0) and (0,1), exhibited almost the same *IV* curves. Since this was also seen for the pristine Bi_2Se_3 LEED patterns, it probably comes from the fact that there are twin domains on the surface that are related by a 180° rotation. The superposition of the two domains should lead to the apparent 2-fold symmetry. Taking this double-domain surface into account, we took the average of the *IV* curves both in the calculation and in the experimental data such that {*h*,*k*} is the average of (*h*,*k*) and (*k*,*h*) spots (see Figure 2a). Note that spots having the same mirror indices of *h* and *k* do not need averaging.

For the SQUID measurements, the fabricated samples were capped with ∼15 nm of Se before taking it out of the UHV chamber, and a commercial MPMS-52 system (Quantum Design) was used. The diamagnetic contribution of the Si substrate was derived from the field-dependent magnetization curves at room temperature and subtracted from all data.

XMCD measurements were performed at BL-4B of UVSOR-III with circularly polarized X-ray radiation (positive helicity with the polarization of 0.6) at 7.2 K and a magnetic field as high as ±5 T was applied to the sample.[39] Instead of changing the photon polarization, we reversed the direction of the magnetic field to derive the XMCD spectra. As shown in Figure 4c, + (−) magnetic field corresponds to the direction antiparallel (parallel) to the direction of the photon incidence. The measurements were first performed for the samples with Se-capping. After measuring, the Se-capped samples were annealed at ∼240 °C to remove the capping layers. LEED observations showed a clear recovery of the 1 × 1 surface periodicity for the cap-removed samples.

For structural optimization and electronic band calculations we used the Vienna Ab Initio Simulation Package[40,41] with generalized gradient approximation (GGA-PBE)[42] to the exchange-correlation potential. The interaction between the ion cores and valence electrons was described by the projector augmented-wave method.[43,44] The Hamiltonian contains scalar relativistic corrections, and the spin−orbit interaction (SOI) is taken into account by the second variation method.[45] To correctly describe the highly correlated Mn-d electrons we include the correlation effects within the GGA+U method.[46] The in-plane lattice constant of the heterostructure was fixed to that of Bi_2Se_3. DFT-D3 van der Waals corrections[47] were applied for accurate structure optimization. The Chern number was calculated for a symmetric $MnBi_2Se_4$/5QL-Bi_2Se_3/

DOI: 10.1021/acs.nanolett.7b00560
Nano Lett. 2017, 17, 3493−3500

$MnBi_2Se_4$ slab by using the method based on tracking the evolution of hybrid Wannier functions realized in Z2 Pack.[48]

■ ASSOCIATED CONTENT

Supporting Information

The Supporting Information is available free of charge on the ACS Publications website at DOI: 10.1021/acs.nanolett.7b00560.

Additional details on ARPES, SARPES, *ab inito* calculations, SQUID, and XMCD measurements (PDF)

■ AUTHOR INFORMATION

Corresponding Author

*E-mail: hirahara@phys.titech.ac.jp. Phone: +81 (0)3 5734 2365. Fax: +81 (0)3 5734 2365.

ORCID

Toru Hirahara: 0000-0002-2574-1708

Sergey V. Eremeev: 0000-0002-9477-3017

Tetsuroh Shirasawa: 0000-0001-5519-6977

Present Addresses

(T.S.) National Institute of Advanced Industrial Science and Technology, Ibaraki 305-8560, Japan.

(T.H.) Department of Crystalline Materials Science, Nagoya University, Nagoya 464-8603, Japan.

(M.M.) Energy Materials Laboratory, Toyota Technological Institute, Nagoya 468-8511, Japan.

(S.K.) Graduate School of Frontier Biosciences and Department of Physics, Osaka University, Suita 565-0871, Japan.

Notes

The authors declare no competing financial interest.

■ ACKNOWLEDGMENTS

The authors thank A. V. Matetskiy, A. A. Saranin, O. Rader, and A. Kimura for discussions. This work has been supported by Grants-In-Aid from Japan Society for the Promotion of Science (Nos. 15H05453, 16K13683, 19340078, and 23244066), the Toray Science Foundation, the Basque Country Government, Departamento de Educación, Universidades e Investigación (Grant No. IT-756-13), the Spanish Ministry of Science and Innovation (Grant Nos. FIS2010-19609-C02-01, FIS2013-48286-C02-02-P, and FIS2013-48286-C02-01-P), the Tomsk State University Academic D.I. Mendeleev Fund Program (Grant No. 8.1.05.2015), and Saint Petersburg State University (project 15.61.202.2015). The ARPES experiments were performed under the UVSOR Proposal Nos. 25-808, 26-531, 27-533, 28-526, and S-15-MS-0034, and the SARPES experiments were performed under the HiSOR Proposal No. 15-A-14. The XMCD measurements were performed under the UVSOR proposal number S-16-MS-2017. The LEED measurements were performed under the ISSP Proposal number H17-A250. The SQUID measurements were performed using facilities of the Cryogenic Research Center, the University of Tokyo. Calculations were performed on the SKIF-Cyberia supercomputer at the National Research Tomsk State University.

■ REFERENCES

(1) https://www.nobelprize.org/nobel_prizes/physics/laureates/2016/.

(2) Hasan, M. Z.; Kane, C. L. Colloquium: Topological insulators. *Rev. Mod. Phys.* **2010**, *82*, 3045.

(3) Qi, X.-L.; Zhang, S.-C. Topological insulators and superconductors. *Rev. Mod. Phys.* **2011**, *83*, 1057.

(4) Qi, X.-L.; Li, R.; Zang, J.; Zhang, S.-C. Inducing a Magnetic Monopole with Topological Surface States. *Science* **2009**, *323*, 1184.

(5) Haldane, F. D. M. Model for a quantum Hall effect without Landau levels: Condensed-matter realization of the parity anomaly. *Phys. Rev. Lett.* **1988**, *61*, 2015.

(6) Qi, X.-L.; Hughes, T. L.; Zhang, S.-C Topological field theory of time-reversal invariant insulators. *Phys. Rev. B: Condens. Matter Mater. Phys.* **2008**, *78*, 195424.

(7) Xu, S.-Y.; et al. Hedgehog spin texture and Berry's phase tuning in a magnetic topological insulator. *Nat. Phys.* **2012**, *8*, 616.

(8) Chang, C.-Z.; et al. Experimental Observation of the Quantum Anomalous Hall Effect in a Magnetic Topological Insulator. *Science* **2013**, *340*, 167.

(9) Bestwick, A. J.; et al. Precise Quantization of the Anomalous Hall Effect near Zero Magnetic Field. *Phys. Rev. Lett.* **2015**, *114*, 187201.

(10) Chang, C.-Z.; et al. High-precision realization of robust quantum anomalous Hall state in a hard ferromagnetic topological insulator. *Nat. Mater.* **2015**, *14*, 473.

(11) Lee, I.; et al. Imaging Dirac-mass disorder from magnetic dopant atoms in the ferromagnetic topological insulator $Cr_x(Bi_{0.1}Sb_{0.9})_{2-x}Te_3$. *Proc. Natl. Acad. Sci. U. S. A.* **2015**, *112*, 1316.

(12) Feng, X.; et al. Thickness Dependence of the Quantum Anomalous Hall Effect in Magnetic Topological Insulator Films. *Adv. Mater.* **2016**, *28*, 6386.

(13) Mogi, M.; et al. Magnetic modulation doping in topological insulators toward higher-temperature quantum anomalous Hall effect. *Appl. Phys. Lett.* **2015**, *107*, 182401.

(14) Qi, S.; et al. High-Temperature Quantum Anomalous Hall Effect in n-p Codoped Topological Insulators. *Phys. Rev. Lett.* **2016**, *117*, 056804.

(15) Chang, C.-Z.; et al. Thin Films of Magnetically Doped Topological Insulator with Carrier-Independent Long-Range Ferromagnetic Order. *Adv. Mater.* **2013**, *25*, 1065.

(16) Sessi, P.; et al. Dual nature of magnetic dopants and competing trends in topological insulators. *Nat. Commun.* **2016**, *7*, 12027.

(17) Sànchez-Barriga, J.; et al. Nonmagnetic band gap at the Dirac point of the magnetic topological insulator $(Bi_{1-x}Mn_x)_2Se_3$. *Nat. Commun.* **2016**, *7*, 10559.

(18) Shiomi, Y.; et al. Spin-Electricity Conversion Induced by Spin Injection into Topological Insulators. *Phys. Rev. Lett.* **2014**, *113*, 196601.

(19) Rojas-Sánchez, J.-C.; et al. Spin to Charge Conversion at Room Temperature by Spin Pumping into a New Type of Topological Insulator: α-Sn Films. *Phys. Rev. Lett.* **2016**, *116*, 096602.

(20) Wang, H.; et al. Surface-State-Dominated Spin-Charge Current Conversion in Topological-Insulator-Ferromagnetic-Insulator Heterostructures. *Phys. Rev. Lett.* **2016**, *117*, 076601.

(21) Wei, P.; Katmis, F.; Assaf, B. A.; Steinberg, H.; Jarillo-Herrero, P.; Heiman, D.; Moodera, J. S. Exchange-Coupling-Induced Symmetry Breaking in Topological Insulators. *Phys. Rev. Lett.* **2013**, *110*, 186807.

(22) Eremeev, S. V.; Men'shov, V. N.; Tugushev, V. V.; Chulkov, E. V. Interface induced states at the boundary between a 3D topological insulator Bi_2Se_3 and a ferromagnetic insulator EuS. *J. Magn. Magn. Mater.* **2015**, *383*, 30.

(23) Katmis, F.; et al. A high-temperature ferromagnetic topological insulating phase by proximity coupling. *Nature* **2016**, *533*, 513.

(24) Eremeev, S. V.; Men'shov, V. N.; Tugushev, V. V.; Echenique, P. M.; Chulkov, E. V. Magnetic proximity effect at the three-dimensional topological insulator/magnetic insulator interface. *Phys. Rev. B: Condens. Matter Mater. Phys.* **2013**, *88*, 144430.

(25) Matetskiy, A. V.; et al. Direct observation of a gap opening in topological interface states of $MnSe/Bi_2Se_3$ heterostructure. *Appl. Phys. Lett.* **2015**, *107*, 091604.

(26) Hsieh, D.; et al. A tunable topological insulator in the spin helical Dirac transport regime. *Nature* **2009**, *460*, 1101.

DOI: 10.1021/acs.nanolett.7b00560
Nano Lett. 2017, 17, 3493−3500

(27) Bianchi, M.; et al. Coexistence of the topological state and a two-dimensional electron gas on the surface of Bi_2Se_3. *Nat. Commun.* **2010**, *1*, 128.
(28) Nowka, C.; et al. Chemical vapor transport and characterization of $MnBi_2Se_4$. *J. Cryst. Growth* **2017**, *459*, 81.
(29) Menshchikova, T. V.; Otrokov, M. M.; Tsirkin, S. S.; Samorokov, D. A.; Bebneva, V. V.; Ernst, A.; Kuznetsov, V. M.; Chulkov, E. V. Band Structure Engineering in Topological Insulator Based Heterostructures. *Nano Lett.* **2013**, *13*, 6064.
(30) Thouless, D. J.; Kohmoto, M.; Nightingale, M. P.; den Nijs, M. Quantized Hall Conductance in a Two-Dimensional Periodic Potential. *Phys. Rev. Lett.* **1982**, *49*, 405.
(31) The magnetization curve does not seem to saturating even at 5 T and shows a characteristic somewhat similar to a paramagnetic one. One possible explanation for this is the presence of Mn atoms at substitutional sites that give a paramagnetic contribution.
(32) Chang, C.-Z.; et al. Chemical-Potential-Dependent Gap Opening at the Dirac Surface States of Bi_2Se_3 Induced by Aggregated Substitutional Cr Atoms. *Phys. Rev. Lett.* **2014**, *112*, 056801.
(33) Zhang, G.; et al. Quintuple-layer epitaxy of thin films of topological insulator Bi_2Se_3. *Appl. Phys. Lett.* **2009**, *95*, 053114.
(34) Sakamoto, Y.; Hirahara, T.; Miyazaki, H.; Kimura, S.-I.; Hasegawa, S. Spectroscopic evidence of a topological quantum phase transition in ultrathin Bi_2Se_3 films. *Phys. Rev. B: Condens. Matter Mater. Phys.* **2010**, *81*, 165432.
(35) Zhang, Y.; et al. Crossover of the three-dimensional topological insulator Bi_2Se_3 to the two-dimensional limit. *Nat. Phys.* **2010**, *6*, 584.
(36) Kimura, S.-I.; et al. SAMRAI: A novel variably polarized angle-resolved photoemission beamline in the VUV region at UVSOR-II. *Rev. Sci. Instrum.* **2010**, *81*, 053104.
(37) Okuda, T.; et al. Efficient spin resolved spectroscopy observation machine at Hiroshima Synchrotron Radiation Center. *Rev. Sci. Instrum.* **2011**, *82*, 103302.
(38) Van Hove, M. A.; et al. Automated determination of complex surface structures by LEED. *Surf. Sci. Rep.* **1993**, *19*, 191.
(39) Nakagawa, T.; Takagi, Y.; Matsumoto, Y.; Yokoyama, T. Enhancements of Spin and Orbital Magnetic Moments of Sub-monolayer Co on Cu(001) Studied by X-ray Magnetic Circular Dichroism Using Superconducting Magnet and Liquid He Cryostat. *Jpn. J. Appl. Phys.* **2008**, *47*, 2132.
(40) Kresse, G.; Hafner, J. *Ab initio* molecular dynamics for open-shell transition metals. *Phys. Rev. B: Condens. Matter Mater. Phys.* **1993**, *48*, 13115.
(41) Kresse, G.; Furthmüller, J. Efficient iterative schemes for *ab initio* total-energy calculations using a plane-wave basis set. *Phys. Rev. B: Condens. Matter Mater. Phys.* **1996**, *54*, 11169.
(42) Perdew, J. P.; Burke, K.; Ernzerhof, M. Generalized gradient approximation made simple. *Phys. Rev. Lett.* **1996**, *77*, 3865.
(43) Blöchl, P. E. Projector augmented-wave method. *Phys. Rev. B: Condens. Matter Mater. Phys.* **1994**, *50*, 17953.
(44) Kresse, G.; Joubert, D. From ultrasoft pseudopotentials to the projector augmented-wave method. *Phys. Rev. B: Condens. Matter Mater. Phys.* **1999**, *59*, 1758.
(45) Koelling, D. D.; Harmon, B. N. A technique for relativistic spin-polarised calculations. *J. Phys. C: Solid State Phys.* **1977**, *10*, 3107.
(46) Liechtenstein, A. I.; Anisimov, V. I.; Zaanen, J. Density-functional theory and strong interactions: Orbital ordering in Mott-Hubbard insulators. *Phys. Rev. B: Condens. Matter Mater. Phys.* **1995**, *52*, R5467.
(47) Grimme, S.; Antony, J.; Ehrlich, S.; Krieg, H. A consistent and accurate ab initio parametrization of density functional dispersion correction (DFT-D) for the 94 elements H-Pu. *J. Chem. Phys.* **2010**, *132*, 154104.
(48) Soluyanov, A. A.; Vanderbilt, D. Computing topological invariants without inversion symmetry. *Phys. Rev. B: Condens. Matter Mater. Phys.* **2011**, *83*, 235401.

DOI: 10.1021/acs.nanolett.7b00560
Nano Lett. 2017, 17, 3493−3500

Supplementary material "A large-gap magnetic topological heterostructure formed by subsurface incorporation of a ferromagnetic layer"

Toru Hirahara,[*,†] Sergey V. Eremeev,[‡,¶,§,‖] Tetsuroh Shirasawa,[⊥,§§] Yuma Okuyama,[†] Takayuki Kubo,[#] Ryosuke Nakanishi,[#] Ryota Akiyama,[#] Akari Takayama,[#] Tetsuya Hajiri,[@,‖‖] Shin-ichiro Ideta,[@] Masaharu Matsunami,[@,⊥⊥] Kazuki Sumida,[△] Koji Miyamoto,[▽] Yasumasa Takagi,[††] Kiyohisa Tanaka,[@] Taichi Okuda,[▽] Toshihiko Yokoyama,[††] Shin-ichi Kimura,[@,##] Shuji Hasegawa,[#] and Evgueni V. Chulkov[‖,‡‡,¶¶,¶,§]

†*Department of Physics, Tokyo Institute of Technology, Tokyo 152-8551, Japan*
‡*Institute of Strength Physics and Materials Science, Tomsk, 634055, Russia*
¶*Tomsk State University, Tomsk, 634050, Russia*
§*Saint Petersburg State University, Saint Petersburg, 198504, Russia*
‖*Donostia International Physics Center (DIPC), Paseo de Manuel Lardizabal, 4, 20018 San Sebastián/Donostia, Basque Country, Spain*
⊥*Institute for Solid State Physics, University of Tokyo, Kashiwa 277-8581, Japan*
#*Department of Physics, University of Tokyo, Tokyo 113-0033, Japan*
@*UVSOR Facility, Institute for Molecular Science, Okazaki 444-8585, Japan*
△*Graduate School of Science, Hiroshima University, Higashi-Hiroshima 739-8526, Japan*
▽*Hiroshima Synchrotron Radiation Center, Hiroshima University, Higashi-Hiroshima 739-8526, Japan*
††*Department of Materials Molecular Science, Institute for Molecular Science, Okazaki 444-8585, Japan*
‡‡*Departamento de Física de Materiales, Facultad de Ciencias Químicas, UPV/EHU, Apdo. 1072, 20080 San Sebastián, Basque Country, Spain*
¶¶*Centro de Física de Materiales, CFM-MPC, Centro Mixto CSIC-UPV/EHU, Apdo.1072, 20080 San Sebastián/Donostia, Basque Country, Spain*
§§*Present address: National Institute of Advanced Industrial Science and Technology, Ibaraki 305-8560, Japan*
‖‖*Present address: Department of Crystalline Materials Science, Nagoya University, Nagoya 464-8603, Japan*
⊥⊥*Present address: Energy Materials Laboratory, Toyota Technological Institute, Nagoya 468-8511, Japan*
##*Present address: Graduate School of Frontier Biosciences and Department of Physics, Osaka University, Suita 565-0871, Japan*

E-mail: hirahara@phys.titech.ac.jp
Phone: +81 (0)3 5734 2365. Fax: +81 (0)3 5734 2365

In this supplementary information, we show sets of data and discussion that are complementary to those shown in the main text.

Band dispersion of the heterostructure measured with different photon energies

Figure S1 shows the band dispersion image of the $MnBi_2Se_4/Bi_2Se_3$ heterostructure taken with different photon energies as well as at different intervals after the sample fabrication. The red lines are the energy distribution curves (EDCs) at the $\bar{\Gamma}$ point to show the size of the gap. It changes with different measurement conditions, but is not relevant to the Dirac-cone position, which becomes gradually deeper by cooling down the sample after sample preparation. One can also see that the Dirac-cone peaks become very weak after 21 hours even for the same measurement condition by comparing Fig. 1(b) and Fig. S1(c).

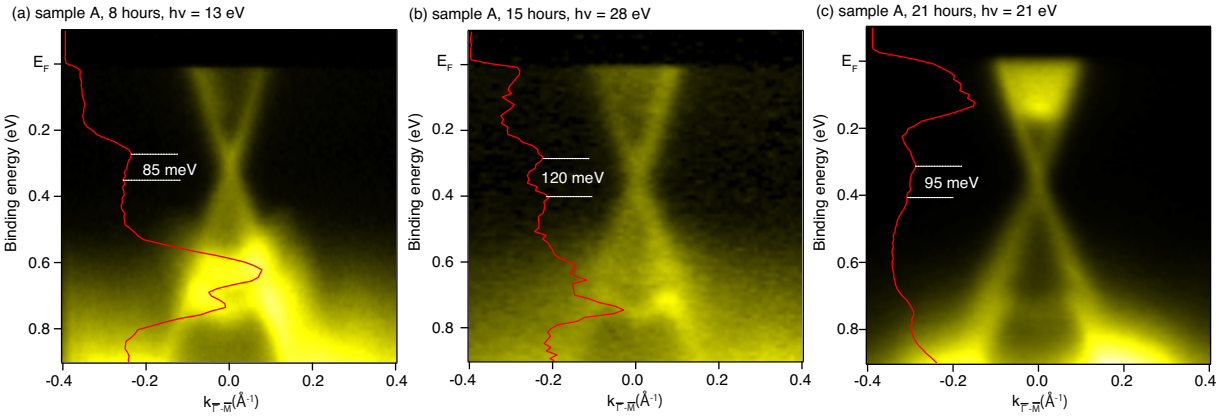

Figure S1: (a) Band dispersion of the $MnBi_2Se_4/Bi_2Se_3$ heterostructure for sample A measured along the $\bar{\Gamma} - \bar{M}$ direction. The spectra was measured 8 hours after cooling down the sample and the APRES measurements were started. The red lines are the energy distribution curves (EDCs) at the $\bar{\Gamma}$ point. The incident photon energy was $h\nu = 13$ eV and the gap size is 85 meV. (b) Same as (a) but measured after 15 hours. The incident photon energy was $h\nu = 28$ eV and the gap size is 120 meV. (c) Same as (a) but measured after 21 hours. The incident photon energy was $h\nu = 21$ eV and the gap size is 95 meV. All the measurements were performed at 30 K.

Band dispersion of the heterostructure measured at room temperature

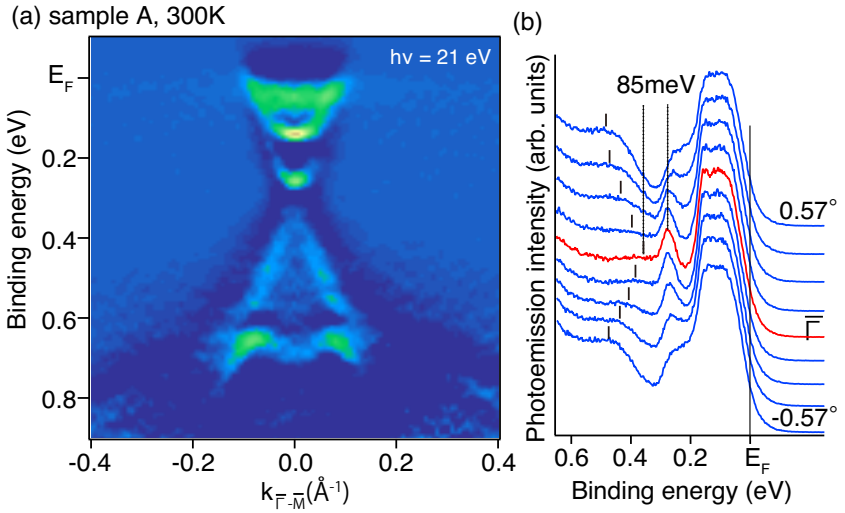

Figure S2: (a) The second derivative of the band dispersion at 300 K of the heterostructure for sample A measured along the $\bar{\Gamma} - \bar{\mathrm{M}}$ direction taken at $h\nu = 21$ eV. (b) Raw spectra (EDCs) near the $\bar{\Gamma}$ point of the band dispersion in (a). The gap size of the Dirac cone is 85 meV.

The gap opening in the Dirac cone was also observed at 300 K, as shown in the band dispersion image in Fig. S2 (a), which was taken before cooling down sample A. The raw spectra (EDCs) are shown in Fig. S2 (b). Although the peak intensity for the lower Dirac branch becomes quite weak, we notice that there is no band crossing and the gap size is estimated as 85 meV. Thus the Curie temperature for the heterostructure is confirmed to be above room temperature also from the ARPES data, and the $MnBi_2Se_4$ SL possesses different magnetic properties compared to that of the bulk $MnBi_2Se_4$. This may be due to the different crystal structure, finite-size effect, or the interface effect. In fact, it has been reported that the magnetic properties at the interface formed by Bi_2Se_3 and EuS are different from those at the interior.[1] Namely, whereas the EuS film prefers in-plane magnetization, the out-of-plane magnetization is favored at the interface and persists up to room temperature, which was explained as due to the large spin-orbit interaction and the spin-momentum locking of the

topological insulator surface. Such effect may also be playing a crucial role in the present system to enhance the Curie temperature.

Band dispersion of the free-standing $MnBi_2Se_4$ septuple layer

Figure S3 shows the calculated band dispersion for the free-standing $MnBi_2Se_4$ septuple layer (SL) along the $\bar{K} - \bar{\Gamma} - \bar{M}$ direction. It is an indirect-gap semiconductor with a gap of ~ 0.4 eV, and the direct gap at the $\bar{\Gamma}$ point is ~ 1 eV.

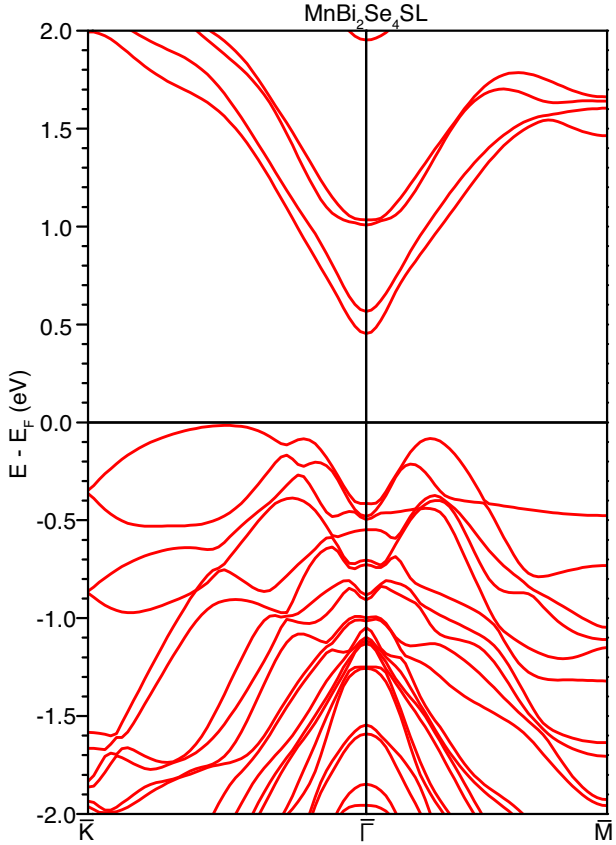

Figure S3: Calculated band dispersion of the free-standing $MnBi_2Se_4$ septuple layer.

$\bar{\Gamma}$ gap dependence on the spin-orbit interaction strength

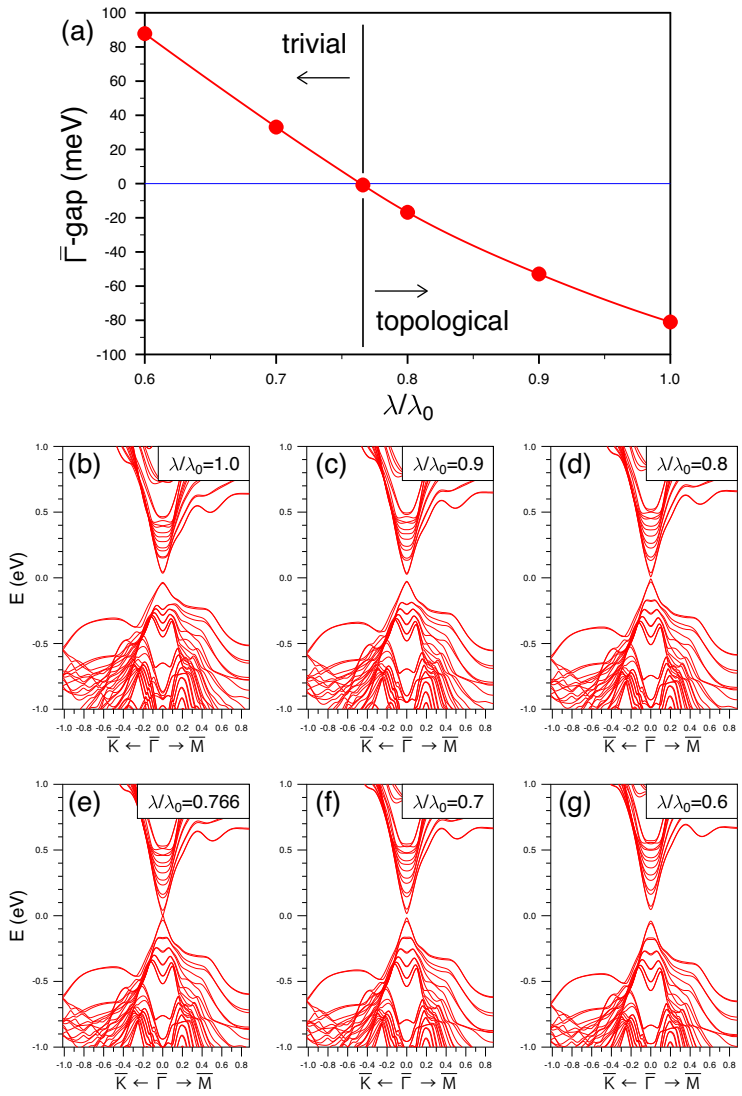

Figure S4: (a) The dependence of the $\bar{\Gamma}$ gap in the $MnBi_2Se_4/Bi_2Se_3$ heterostructure on the relative spin-orbit interaction strength λ/λ_0. (b)-(g) Band dispersion of the heterostructure for various spin-orbit coupling strengths (λ/λ_0 is 1.0 (b), 0.9 (c), 0.8 (d), 0.766 (e), 0.7 (f), and 0.6 (g), respectively).

Figure S4 (a) shows the calculated dependence of the gap at the $\bar{\Gamma}$ point of the $MnBi_2Se_4/Bi_2Se_3$ heterostructure on the relative spin-orbit interaction (SOI) strength λ/λ_0 where λ_0 is its actual value. Red points are calculated values and the red line is a guide for eyes. The negative/positive gap corresponds to topological non-trivial/trivial quantum phase. Zero

gap is the topological quantum phase transition point. Figures S4(b)-(g) show the actual calculated band dispersions that have been used to derive the gap size shown in Fig. S4 (a). The gap in Fig. S4 is the $\bar{\Gamma}$ gap in the symmetric slab spectrum and not in the bulk one. At the $\lambda/\lambda_0 = 1.0$ limit, it corresponds to the gap in the surface Dirac state as discussed in the main text (see Fig. 3). Note that at $\lambda = \lambda_0$, the system has two types of gap: the inverted bulk gap of the Bi_2Se_3 and the inverted surface state gap inside the bulk one. At the beginning of the SOI decrease with respect to its real value (λ_0), the edges of the bulk gap are located relatively far from the surface state gap edges and cannot directly contribute to the gap narrowing (see Fig. 3(a)). Then, when the SOI is getting weaker the bulk inverted gap becomes narrower. As a consequence, the gapped Dirac state becomes less localized at the surface and respectively leads to weaker interaction of the surface state with the Mn atomic layer that finally results in the surface state gap narrowing. At $\lambda/\lambda_0 = 0.8$, the gap edges at $\bar{\Gamma}$ have almost no surface localization and at $\lambda/\lambda_0 = 0.766$, we find that the gap closes (topological phase transition). Further decrease in the SOI results in reopening of the gap in the bulk spectrum (now it is non-inverted or normal gap) without any surface state within this gap.

XMCD measurements on Se-capped samples

In order to check if the magnetic properties are affected by the Se capping, we performed XMCD measurements with the capping layer on top of the heterostructure prior to removing it. Figure S5 shows the X-ray absorption spectra (XAS) together with the XMCD spectrum at the Mn absorption edge. μ_+ and μ_- correspond to the spectrum obtained at $+5$ T and -5 T, respectively. There is a linear background due to the capping layer. Comparing Fig. 4(a) and Fig. S5, we observe the XMCD signal for the L_3 edge in both cases although it is weak in Fig. S5, possibly due to the dominant contribution from the capping layer. Thus we can say that the capping layer has little effect on the magnetic properties of the

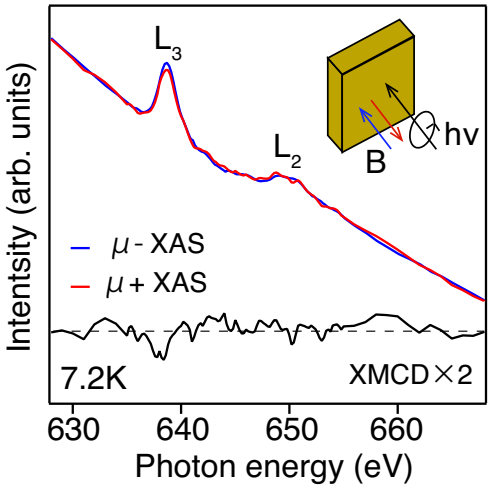

Figure S5: X-ray absorption spectra (XAS) at 7.2 K for a circularly polarized incident light when a ±5 T magnetic field was applied along the surface-normal direction. μ_+ and μ_- correspond to the spectrum obtained at +5 T and −5 T, respectively. The corresponding XMCD spectra is also shown. The measurements were performed with the Se capping layer on top of the heterostructure prior to its removal in UHV.

heterostructure and although the surface sensitivity is different between SQUID and XMCD, we believe that they are probing the same magnetization since the Mn layer is the only one that can show magnetism in this heterostructure.

Derivation of the magnetic moment based on the sum-rule analysis

Figure S6 (a) shows the XAS measured at 7.2 K for a circularly polarized incident light when a ±5 T magnetic field was applied at an angle of 55° with respect to the sample normal after the removal of the Se capping layer in UHV. μ_+ and μ_- correspond to the spectrum obtained at +5 T and −5 T, respectively. In this case, the magnetic field has both out-of-plane and in-plane components. Since the angle between the light-incidence and surface-normal is 55° which is the magic angle that the contribution of the intra-atomic dipolar moment vanishes, we can deduce the angle-independent spin magnetic moment by using the sum rule[2] (assuming the hole number as 5 for Mn) and the result is $m_{spin} = (1.99 \pm 0.21)\mu_B$. This value

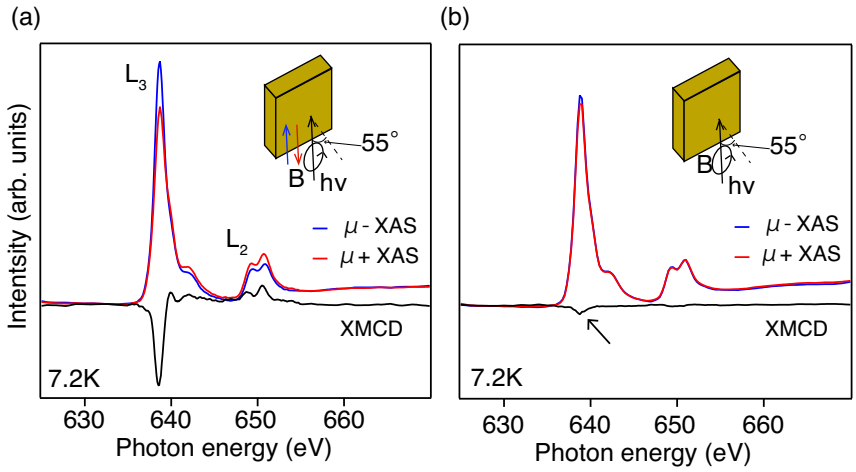

Figure S6: (a) X-ray absorption spectra (XAS) at 7.2 K for a circularly polarized incident light when a ±5 T magnetic field was applied. The angle between the surface normal and the magnetic field is 55°. The corresponding XMCD spectrum is also shown. The Se capping layer was removed by annealing the sample in UHV. (b) Same as (a) but measured at zero tesla. A remanent XMCD signal can be observed.

was deduced considering the polarization of the incident X-rays ($P = 0.6$) and also corrected using the correlation factor ($C = 0.68$) of Mn^{2+} considering the L_3 and L_2 edge overlap.[3–5] Similarly, the orbital magnetic moment is calculated as $m_{orbital} \sim (-0.02 \pm 0.04)\mu_B$. Thus the experimentally determined magnetic moment of Mn in the heterostructure at 5 T is $m_{spin} \sim 1.99\mu_B$ and smaller than that of the first-principles calculation ($4.61\mu_B$). This shows that we need a larger magnetic field to fully saturate the magnetization. Since the ratio of $m_{orbital}$ and m_{spin} is $m_{orbital}/m_{spin} \sim -0.01$, we believe that the Mn atoms in the heterostructure are in the high spin state ($S = 5/2, L = 0$).

Figure S6(b) shows the XMCD data at remanence. As in the case shown in Fig. 4(d), the XMCD signal is weakly observed at the L_3 edge and this shows that the system is ferromagnetic. These results again show that the Se-capping does not have any influence on the magnetic properties of the heterostructure.

SQUID measurements for in-plane magnetization

Figures S7(a) and (b) show the magnetization curves measured with SQUID for the Se-capped sample B when the magnetic field was applied in the surface-parallel direction (x direction in Fig. S8 (c)) at 4 K and at 300 K, respectively. The inset shows the close-up for -0.1 to 0.1 T, and one can see clear hysteresis loops, meaning that the $MnBi_2Se_4/Bi_2Se_3$ heterostructure can be magnetized also in the surface-parallel direction even at room temperature. However the residual magnetization is small compared to the saturation value which is the same as that for the out-of-plane magnetized case.

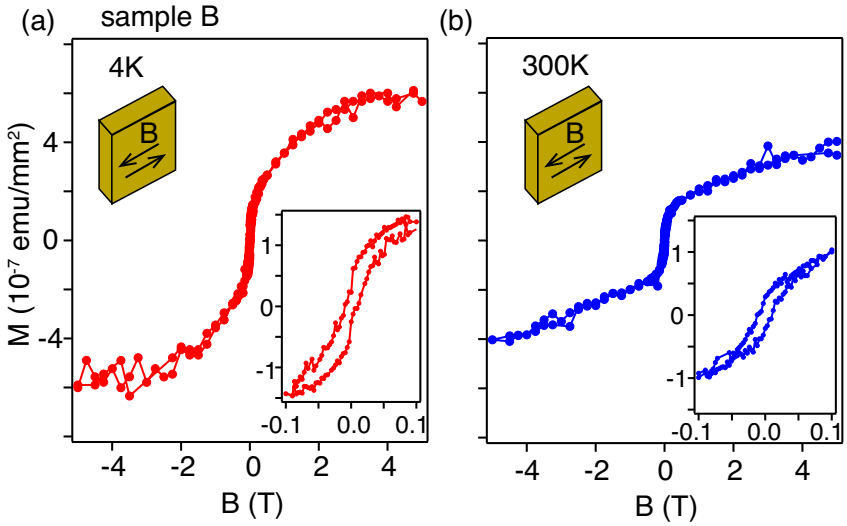

Figure S7: (a),(b) Magnetization curves measured with SQUID for the Se-capped sample B taken at 4 K (a) and at 300 K (b), respectively. The magnetic field was applied parallel to the sample surface. The inset shows the close-up near zero-field. Clear hysteresis loops can be observed both at 4 K and 300 K.

Spin- and angle-resolved photoemission measurements

Figure S8 shows the detailed data set of the spin and angle-resolved photoemission spectroscopy (SARPES) measurements for the massive Dirac cone of the $MnBi_2Se_4/Bi_2Se_3$ heterostructure. The band dispersion does not change before (Fig. S8(a)) and after (Fig. S8(b)) a magnetic field as large as $\sim$0.1 T was applied perpendicular to the surface. Figure S8(c) shows

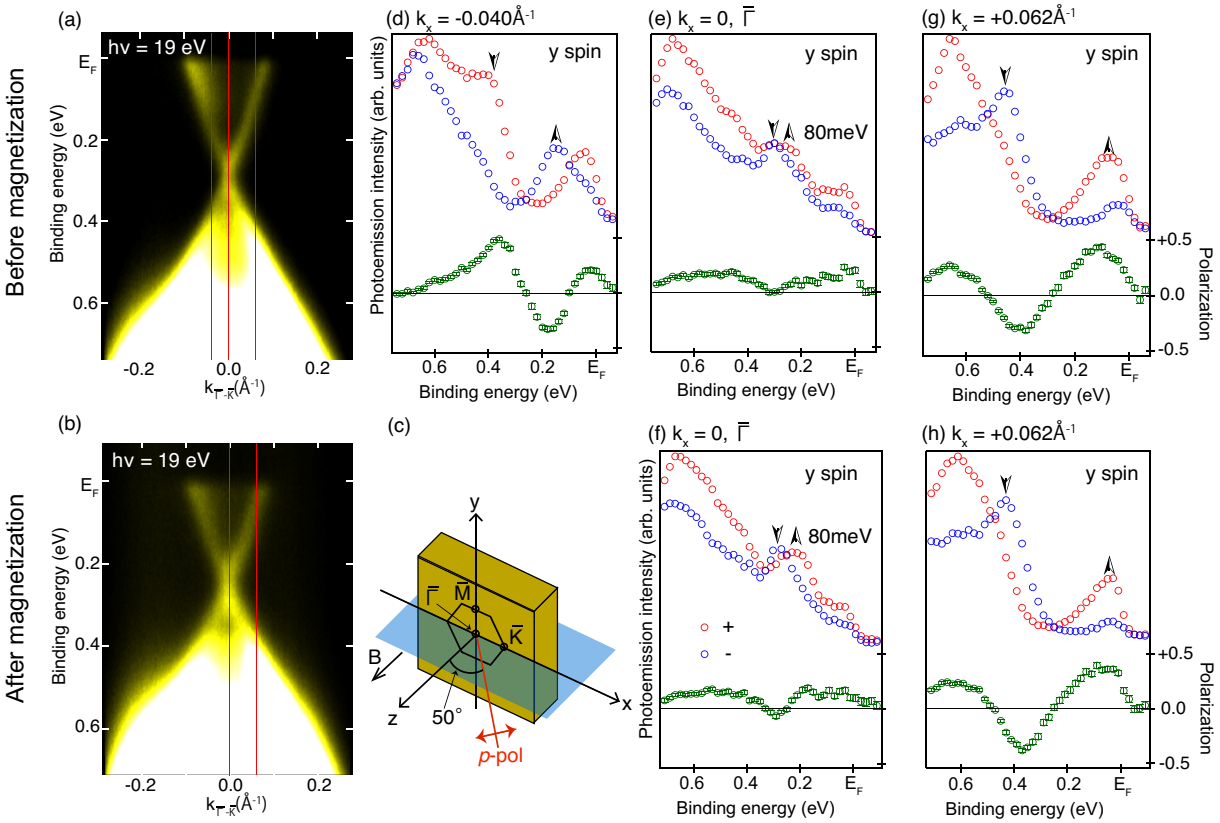

Figure S8: (a, b) Band dispersion image of the $MnBi_2Se_4/Bi_2Se_3$ heterostructure taken before (a) and after (b) a magnetic field as large as ∼0.1 T was applied in the sample surface normal (z) direction, respectively. The incident photon energy was $h\nu = 19$ eV and the gap size is 80 meV. The red lines indicate the wavenumbers where the spin and angle-resolved photoemission (SARPES) measurements were performed. (c) The experimental geometry of the present SARPES measurement. (d) SARPES data at $k_x = -0.040^{-1}$ for the y spin component before the sample was magnetized. The Dirac-cone states are shown by the arrow pointing up and down. (e) Same as (d) but for $k_x = 0$. (f) Same as (e) but after the magnetic field was applied. (g) Same as (d) and (e) but for $k_x = +0.062^{-1}$. (h) Same as (g) but after the magnetic field was applied.

the experimental geometry and the definition of the coordinates in the present SARPES measurement. Figures S8(d) and (g) shows a clear signature of the expected in-plane spin-momentum locking of the helical Dirac cone. At the $\bar{\Gamma}$ point (Fig. S8(e)), the gapped Dirac can be distinguished clearly from the SARPES spectra. However, it shows finite positive y spin-polarization for nearly the whole energy region even though it should show no spin-polarization in principle. We believe this is due to spin-dependent photoemission dipole matrix element (SME), which has been reported previously for a similar experimental condition.[6,7] This is also supported by the fact that the spin-polarization values for the states with $+y$ spin have larger values than those with $-y$ spin (Figs. S8(d) and (g)), meaning that there is a positive background due to the SME.[6,7] After the magnetization, the lower gapped Dirac state becomes a bit negatively polarized as can be seen in Fig. S8 (f). However, the signal is small and since the shape of the spin-polarization curve does not change between Figs. S8(e) and (f), we believe that it likely has no significant meaning. We have applied the field along the z-direction and it seems unreasonable to expect an enhancement in the y polarization.

Theory also predicts that as a result of the out-of-plane magnetization, an out-of-plane spin polarization is expected at the gapped Dirac points. We have performed SARPES measurements to detect this spin polarization in the z direction and the results are shown in Fig. S9. Figure S9(a) shows the band dispersion image along the along the $\bar{\Gamma} - \bar{\mathrm{K}}$ direction taken at $h\nu = 20$ eV. The arrow shows the "Mn" band described in Fig. 3(a). The red and blue circles in Figs. S9(b)-(d) show the data for $+z$ and -z spins, and the green circles show the spin-polarization curves with error bars. The spectra of Figs. S9(b), (d), (f) are those obtained without applying any magnetic field, and those shown in Figs. S9(c), (e), (g) are the ones obtained after application of a magnetic field of $\sim$0.1 T perpendicular to the surface at room temperature for different wavenumbers. From Fig. 4 (b), the hysteresis loop closes at 0.05 T at 300 K. Thus 0.1 T should be sufficient to magnetize the sample. Before magnetization, no S_z was observed as shown in Fig. S9(b).

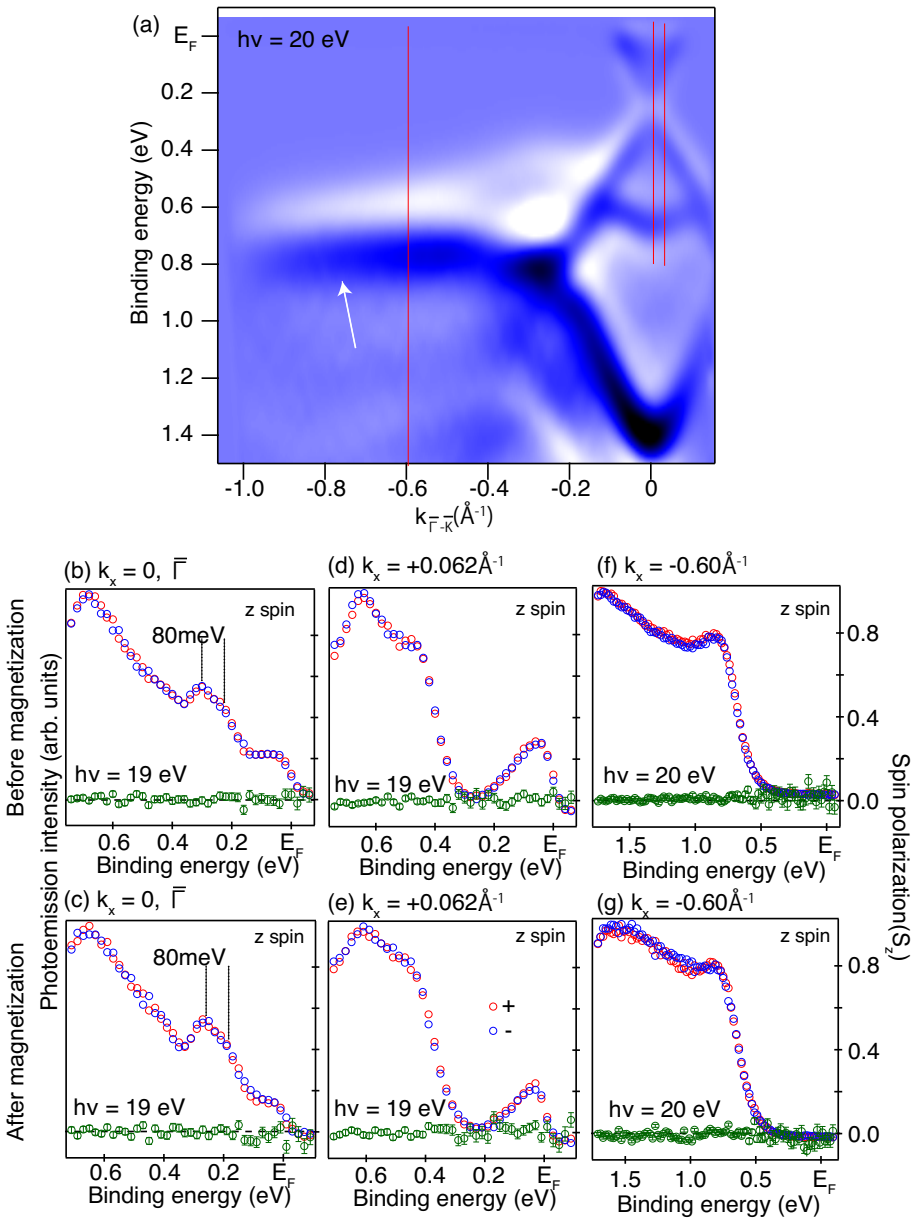

Figure S9: (a) Band dispersion image (second derivative) of the $MnBi_2Se_4/Bi_2Se_3$ heterostructure along the $\bar{\Gamma} - \bar{K}$ direction taken at $h\nu = 20$ eV. The arrow shows the "Mn" band described in Fig. 3(a). The red lines indicate the wavenumbers where the spin and angle-resolved photoemission (SARPES) measurements were performed. (b) SARPES data at $k_x = 0$ for the z spin component before the sample was magnetized taken at $h\nu = 19$ eV. (c) Same as (b) but after the sample was magnetized. (d) Same as (b) but for $k_x = +0.062^{-1}$. (e) Same as (d) but after sample was magnetized. (f) SARPES data at $k_x = -0.60^{-1}$ for the z spin component before the sample was magnetized taken at $h\nu = 20$ eV. (g) Same as (f) but after the sample was magnetized.

According to the calculations, the out-of-plane components of the spin-expectation values S_z are 0.324 and -0.421 for the lower and upper branches of the gapped Dirac state at the $\bar{\Gamma}$ point, respectively. However, we did not observe a prominent S_z even when the sample was magnetized, as shown in Fig. S9(c), and it was nearly zero within the error bars. This can be explained as follows. The expected out-of-plane spin-polarization written above assumes a magnetic moment of 4.61 μ_B for the Mn layer which is the case when the heterostructure is fully magnetized. In the experiment, the spin magnetic moment of the Mn atoms deduced from the XMCD measurement is 1.99 μ_B with negligible contribution from the orbital magnetic moments as written above. Thus considering the fact that the residual magnetization at 0 T is 4∼7 % as that at 5 T (Figs. 4(b), (d)), we can only expect $S_z \sim 0.008$ for the Dirac cone assuming that the observed S_z in the experiment should be proportional to the magnetic moment of the Mn atoms. This is smaller than the values of the error bars of spin-polarization (±1.5 %) in Fig. S9(c). Thus the experimentally measurable S_z for the gapped Dirac cone is below the detection limit.

We have also performed SARPES measurements for the "Mn" band which directly reflects the magnetization of $MnBi_2Se_4$, as shown in Fig. S9(g). Before magnetization, no S_z was observed as shown in Fig. S9(f). The calculation predicts $S_z = 0.638$ for this state so we can expect $S_z \sim 0.012$ in the experiment. Again, this is smaller than the error bars in Fig. S9(g) of ±1.5 % and we could not observe a prominent out-of-plane spin polarization even after magnetizing the sample. Thus it is really difficult to show the finite S_z in the band structure in the present system due to the extremely small residual magnetization, although it is clear that the system is ferromagnetic. Since the magnetic layer is a monolayer of Mn and thus ultrathin, it is difficult to maintain the single-domain structure and easily break up into multi-domains when the magnetic field is turned off. Such feature is reported to be common for very thin magnets,[8] and the direct observation of such magnetic domain structure has been shown for the $SrTiO_3$ surface.[9]

The z spin component was not observed for $k_x = +0.062^{-1}$ neither before nor after

application of a magnetic field, as shown in Figs. S9 (d) and (e). This behavior is expected from theory.

Dirac-cone dispersion for various magnetization directions

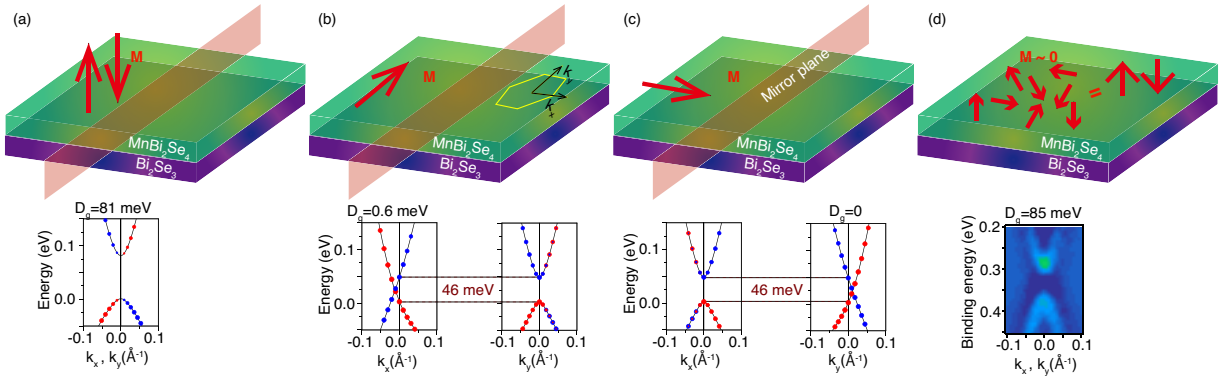

Figure S10: Schematic drawing and the calculated (experimental) band dispersion of the Dirac cone for the $MnBi_2Se_4/Bi_2Se_3$ heterostructure when the magnetization is out-of-plane (a), in-plane and parallel to the mirror plane (b), in-plane and perpendicular to the mirror plane (c), and when the net magnetization is nearly zero due to many domains with random distribution of magnetization (d). In (d), the situation is virtually the same as (a) since the in-plane components of the magnetization are so random that the band-shift effects are canceled out as a whole and only the out-of-plane component dominates.

The clear observation of the Dirac-cone gap in the possible presence of magnetic multi-domains seems puzzling but also intriguing. The heterostructure can actually be ferromagnetic in the in-plane direction, as has been shown by the magnetization curves measured with SQUID in Fig. S7. By comparing Figs. 4(a), (b) and Fig. S7, it is difficult to determine the easy axis experimentally as the characteristics of the magnetization curves are not so different. We believe that the magnetic anisotropy energy is small in this system as also suggested by *ab initio* calculations (only 0.2 meV difference between out-of-plane and in-plane magnetization directions). So the samples should also have magnetic domains pointing in the in-plane direction. When a magnetic field is applied, a single domain spin state is realized, but breaks up into magnetic domains pointing in various directions when it is turned off. The difference before and after the application of a magnetic field should be a slight dominance

of the magnetic domain with the magnetic moment oriented parallel to the applied field, which shows up as the residual magnetization shown in Figs. 4(a)-(d), Fig. S6 and Fig. S7.

So now let us discuss how the band structure is affected for different magnetization directions. As we have discussed previously, when the magnetization of the heterostructure is out-of-plane, the Dirac cone becomes gapped by 81 meV and the dispersion is isotropic (Fig. S10(a)). The dispersion does not change whether the magnetization is $+z$ or $-z$. There are only two possible magnetic orientations that give the same contribution to the band structure. Now if the sample magnetization is in-plane, the situation is completely different. Figures S10(b) and (c) show the dispersion near the Dirac point when the magnetization is parallel (y) and perpendicular (x) to the mirror plane (see Fig. 2(b)) of the heterostructure, respectively. In Fig. S10(b), the Dirac cone is shifted in the $-k_x$ direction by 0.01155 Å^{-1} with a small band gap of 0.6 meV, whereas for k_y, the dispersion is symmetric for the + and − wavenumber directions with a gap of 46 meV at the $\bar{\Gamma}$ point, which is due to the cone shifting. On the other hand in Fig. S10(c), the Dirac cone is shifted in the $+k_y$ direction by 0.01155 Å^{-1} with no band gap, whereas for k_x, the dispersion is symmetric for the + and − wavenumber directions with a gap of 46 meV. The absence of the band gap in the k_y direction is due to the dual topological character of the $MnBi_2Se_4/Bi_2Se_3$ heterostructure. This was clearly shown for the case of Bi_2Te_3[10] and the gap opening is not permitted when the crystal mirror symmetry is not violated since Bi_2Te_3 is a topological crystalline insulator (TCI) as well as a topological insulator. Bi_2Se_3 as well as the heterostructure is also a TCI. In summary, when the magnetization is in-plane, the Dirac cone is shifted in the direction perpendicular to the magnetization direction with anisotropic dispersions. So there are an infinite number of possible orientations of magnetization, each of which gives different contributions to the band structure.

Manipulation of the band structure by changing the magnetization direction has been recently reported[11] for a ferromagnet Fe(001). In the present case, we need to say that although the band structure should change as shown in Fig. S10(a)-(c), the residual magnetization

is so small that we actually could not see any change even after applying the magnetic field in the in-plane direction. So at 0 T, the net magnetization is nearly zero due to the existence of many domains with various directions of magnetization for a realistic sample with a slight dominance of the domain parallel to the applied magnetic field as discussed above (Fig. S10(d)). However, the in-plane components of the magnetization are so random that the band-shift effects are canceled out. In contrast, the out-of-plane components in all domains should give the same contribution and when summed up, give the main contribution. As a result, the situation for $M \sim 0$ is virtually equivalent to the out-of-plane magnetized case and we believe that this is the reason why we observe a clear gap opening even when we cannot obtain a fully out-of-plane magnetized sample. On the other hand, this means that self-assembly permits the formation of a massive Dirac cone in the heterostructure irrespective of the net magnetic state of the sample.

In fact, this kind of situation is similar to the superparamagnetic domain structure found in Cr(Bi, Sb)$_2$Te$_3$.[12] Through spatially-resolved SQUID measurements, the authors have found coexistence of the QAHE and a superparamagnetic behavior associated with magnetic domains that weakly interact with each other and lack long-range order near zero-field. They also observed domains that did not show significant out-of-plane magnetization. Such coexistence of superparamagnetism and the QAHE was also suggested by transport measurements in V(Bi, Sb)$_2$Te$_3$ films.[13] On the other hand, magnetic force microscopy measurements on V-doped Sb_2Te_3 films showed a typical domain behavior of a ferromagnet, that is domain nucleation and domain wall propagation.[14] Thus the correlation among magnetic domains and the QAHE as well as the Dirac-cone gap opening in these systems as well as our heterostructure should be examined further in more detail.

References

(1) Katmis, F. et al. A high-temperature ferromagnetic topological insulating phase by proximity coupling. *Nature* **2016** *533*, 513.

(2) Stöhr, J.; König, H., Determination of Spin- and Orbital-Moment Anisotropies in Transition Metals by Angle-Dependent X-Ray Magnetic Circular Dichroism. *Phys. Rev. Lett.* **1995** *75*, 3748.

(3) Okabayashi, J. et al. Investigating Orbital Magnetic Moments in Spinel-Type MnV_2O_4 Using X-ray Magnetic Circular Dichroism. *J. Phys. Soc. Jpn.* **2015** *84*, 104703.

(4) Teramura, Y.; Tanaka, A.; Jo, T., Effect of Coulomb Interaction on the X-Ray Magnetic Circular Dichroism Spin Sum Rule in 3*d* Transition Elements. *J. Phys. Soc. Jpn.* **1996** *65*, 1053.

(5) Piamonteze, C.; Miedema, P.; de Groot, F. M. F., Accuracy of the spin sum rule in XMCD for the transition-metal *L* edges from manganese to copper. *Phys. Rev. B* **2009** *80*,184410.

(6) Jozwiak, C. et al. Photoelectron spin-flipping and texture manipulation in a topological insulator. *Nature Physics* **2013** *9*, 293 (2013).

(7) Jozwiak, C. et al. Widespread spin polarization effects in photoemission from topological insulators. *Phys. Rev. B* **2011** *84*, 165113.

(8) Johnson, M. T.; Bloemen, P. J.; der Broeder, F. J. A.; de Varies, J. J., Magnetic anisotropy in metallic multilayers. *Rep. Prog. Phys.* **1995** *59*, 1409.

(9) Taniuchi, T. et al. Imaging of room-temperature ferromagnetic nano-domains at the surface of a non-magnetic oxide. *Nature Commun.* **2016** *7*, 11781.

(10) Rauch, T.; Flieger, M.; Henk, J.; Mertig, I.; Ernst, A., Dual Topological Character of Chalcogenides: Theory for Bi_2Te_3. *Phys. Rev. Lett.* **2014** *112*, 016802.

(11) Młyńczak, E. et al. Fermi Surface Manipulation by External Magnetic Field Demonstrated for a Prototypical Ferromagnet. *Phys. Rev. X* **2016** *6*, 041048.

(12) Lachman, E. O. et al. Visualization of superparamagnetic dynamics in magnetic topological insulators. *Sci. Adv.* **2015** **1**, e1500740.

(13) Grauer, S. et al. Coincidence of superparamagnetism and perfect quantization in the quantum anomalous Hall state. *Phys. Rev. B* **2015** *92*, 201304.

(14) Wang, W.; Chang, C.-Z.; Moodera, J. S.; Wu, W., Visualizing ferromagnetic domain behavior of magnetic topological insulator thin films. *npj Quantum Materials* **2016** *1*, 16023.